69th International Astronautical Congress (IAC), Bremen, Germany, 1-5 October 2018.

IAC–18–C1.6.3

Ultra-Soft Electromagnetic Docking with Applications to In-Orbit Assembly

Rebecca C. Foust[a*], **Elena Sorina Lupu**[b], **Yashwanth Kumar Nakka**[c], **Soon-Jo Chung**[d], **and Fred Y. Hadaegh**[e]

[a] *Graduate Student, Aerospace Engineering, University of Illinois at Urbana-Champaign, Urbana, IL, 61801, USA, Special Student, California Institute of Technology, Pasadena, CA, 91125, USA* foust3@illinois.edu
[b] *Research Engineer, GALCIT, California Institute of Technology, Pasadena, CA, 91125, USA,* eslupu@caltech.edu
[c] *Graduate Student, GALCIT, California Institute of Technology, Pasadena, CA, 91125, USA,* yknakka@caltech.edu
[d] *Associate Professor of Aerospace and Bren Scholar; Jet Propulsion Laboratory Research Scientist, California Institute of Technology, Pasadena, CA, 91125, USA,* sjchung@caltech.edu
[e] *Senior Research Scientist and Technical Fellow, Jet Propulsion Laboratory, California Institute of Technology, Pasadena, CA, 91109, USA,* fred.y.hadaegh@jpl.nasa.gov.
* Corresponding Author

Abstract

Docking small satellites in space is a high-risk operation due to the uncertainty in relative position and orientation and the lack of mature docking technologies. This is particularly true for missions that involve multiple docking and undocking procedures like swarm-based construction and reconfiguration. In this paper, an electromagnetic docking system is proposed to mitigate these risks through robust, ultra-soft, propellant-free docking. Designed with reconfigurable self-assembly in mind, the gripping mechanism is androgynous, able to dock at a variety of relative orientations, and tolerant of small misalignments. The mechanical and control design of the system is presented and tested in both simulation and on a fleet of 6 degree-of-freedom (DOF) spacecraft simulators. The spacecraft simulators float on the precision flat floor facility in the Caltech Aerospace Robotics and Control lab, the largest of its kind at any university. The performance of the electromagnetic docking system on-board the simulators is then compared against a propulsive docking system.

Nomenclature

θ	Heading Angle
μ_0	Magnetic Permeability of Free Space
ρ	Density of the Electromagnet Coil Material
σ	Coil Axial Turn Density
B	Control Influence Matrix
N	Number of Windings
T	Array of Thruster Commands
f	Electromagnet Force
h	Coil Separation Distance
i	Current
l	Coil Thickness
m	Electromagnet mass
m_z	Moment about Z-Axis
p	Power Consumption of the Electromagnet
r	Coil Radius
v	Drive Voltage of the Electromagnet

Acronyms/Abbreviations

Degree Of Freedom (DOF), Multi-Spacecraft Testbed for Autonomy Research (M-STAR), Small Satellite (SmallSat), Minimum Impulse Bit (MIB)

1 Introduction

In-orbit self-assembly of a large-scale structure from component satellites would enable several advanced satellite missions like a large, modular space telescope with a mirror diameter that could be increased with the launch of additional satellites or an orbital gateway that can increase in size with increased usage and funding. Since the component satellites could be mass-produced from a small set of different component types, the benefit from economy of scale would reduce the overall mission cost when compared to monolithic satellites. Such a mission architecture also provides increased reliability due to

redundancy, increased flexibility, and the ability to self-repair, which would be beneficial for distant assemblies like telescopes in Lagrange points or lunar gateways.

Autonomous rendezvous and docking (AR&D) technologies for small satellites are necessary to enable in-orbit assembly schemes. SmallSats have the distinct advantages of low cost and weight, which make them particularly attractive to multi-agent missions like in-orbit assembly. With these benefits come restrictions, however. SmallSats have reduced performance across the board, in power generation, computing, pose determination and control. These difficulties are even more pronounced as the size of the satellite is decreased. Nanosatellite and CubeSat scale sensors and actuators are limited in performance and have few options available [1]. The most successful proximity operations CubeSat mission, the CanX-4&5 mission, was able to achieve centimeter-level position determination and sub-meter level control [2]. For a docking mission, this level of accuracy could lead to dock failure or even collision. These sensing and actuation gaps make activities like AR&D much more difficult, but through the use of well-designed controllers and docking actuators these difficulties can be overcome. This paper discusses the use of an electromagnet-based docking system to mitigate the risk of SmallSat AR&D and accommodate the insufficient sensors and actuators in this class of satellites, and compares it against a standard thruster-based docking.

1.1 *SmallSat Docking Literature Review*

Docking systems currently in use for large satellites like the International Space Station can be applied to SmallSats to some extent, but due to the drastic differences in mass, space, and power, rethinking the docking system for SmallSats is a challenging and interesting problem from both research and engineering points of view.

In this paper, ultra-soft docking is defined as a dock where the relative velocity is less than 1 mm/s, soft docking has a relative velocity of less than 1 cm/s, and hard docking is above 1 cm/s.

In literature, several solutions have been proposed to perform docking in space for SmallSats. The main categories include thruster-based docking, tether-based docking, and magnet-based docking. A selection of SmallSat missions involving docking that flew into space or are proposed to fly into space is presented in Table 1.

1.1.1 *Thruster-Based Docking*

Thruster-based docking is the most common form of docking and has a long history of success in space. Thrusters provide the most maneuverability of any of the docking types discussed. With thrusters, the initial separation can be as large as the propellant storage of the satellite allows.

However, thruster-based docking has drawbacks like the propellant consumption. The MIB of the thruster affects the resolution of the maneuver and drives consumption up for precise motion like docking. This also dictates the minimum impact velocity. Thruster-based docking also comes with the risk of thruster plume impingement, which can lead to disturbance forces and undue heating, causing dock and component failure [10, 11, 12]. These limitations can make missions like assembly of a structure difficult.

1.1.2 *Tether-Based Docking*

Tether-based docking is advantageous since it is repeatable and the main spacecraft stay separated until the tether begins to reel, so docking failures can often be fixed with little risk to the main spacecraft. Additionally, with some extra sensors the tether can be used to improve the relative navigation accuracy [13, 14]. Tether-based docking poses disadvantages such as tether entanglement if tension is not maintained, as well as increased complexity in design. However, it is more robust to failure since the tether can be rolled back and a new attempt can be made.

Several studies have examined controlling tethered satellites and docking via tethers, but generally the satellites are launched with the tethers connected [15, 4]. In some concept missions without pretethered satellites, the tether is ejected forcefully to intercept the target like shooting a harpoon gun. To add more flexibility, some studies use an electromagnetic end effector to aide in the capture [16, 17, 18]. While this helps in final capture, it increases complexity, cost, and weight.

1.1.3 *Magnetic Docking*

Magnet-based docking comes in two forms, permanent magnets and electromagnets. The permanent magnets create a hard dock and have a small capture range, but are simple to implement. In [19], permanent magnets are used for the docking mechanism, but the capture range issue is overcome by using thrusters to bring the CubeSats into close proximity.

Electromagnet-based docking can provide a smoother, more accurate docking. In addition, it

Mission Name	Lead Organization	Status	Docking Actuation
AAReST [3]	Caltech and Surrey Space Center	Scheduled for Launch, 2019	Electromagnets
STARS 1 [4]	Kagawa University	Jan. 23, 2009	Pre-Tethered
STARS 2 [5]	Kagawa University	Feb. 28, 2014	Pre-Tethered
CPOD[6]	Tyvak Nano-Satellite Systems	Awaiting Launch	Thrusters
Rascal [7]	St. Louis University	Cancelled	Thrusters
CleanSpace One [8]	EPFL	Gathering Funds	Thrusters
Spheres [9]	MIT	May-November 2006	Thrusters
STRaND 2 [3]	Surrey Space Center	No Information Available	Electromagnets

Table 1: Review of SmallSat Docking Missions

does not require consumables to operate, and does not create plumes. As a disadvantage, more current and thus more mass is required to bring satellites together from longer distances. As superconductor technology improves though, this limitation can be ameliorated. Several studies have suggested electromagnetic docking, in addition to the ARReST and STRaND 2 missions from Table 1, but these docks are typically hard docks to ensure dock completion. Electromagnets have been also studied for formation flying applications, like in references [20], [21], [22], [23], or in contact-free docking applications such as [24].

1.2 *Spacecraft Simulator Facility Overview*

The Caltech Aerospace Robotics and Control Lab's Spacecraft Simulator Facility is composed of an ultra-precise epoxy flat floor shown in Fig. 1, a clean room, and five M-STAR robots. The flat floor facility is the largest such facility at any university. It has two 7DOF robot arms mounted on linear actuators along the back and the side. The space is fully covered by 14 motion capture cameras placed around the exterior to track the position and orientation of each M-STAR.

The M-STARs, shown in Fig. 2, use flat and spherical air bearings to achieve 5DOF frictionless motion and a linear actuator to achieve kinematic motion in the gravity direction. The M-STARs are equipped with thrusters, reaction wheels, electromagnets, and docking ports as actuators. The M-STARs are designed to be modular, capable of transforming from a 6DOF platform to a 3DOF and everything in between. For the purposes of this research, the M-STARS will be in two different 3DOF configurations, one with thrusters and docking ports and one with electromagnets and docking ports.

For more details on the facility and the simulators, see reference [25].

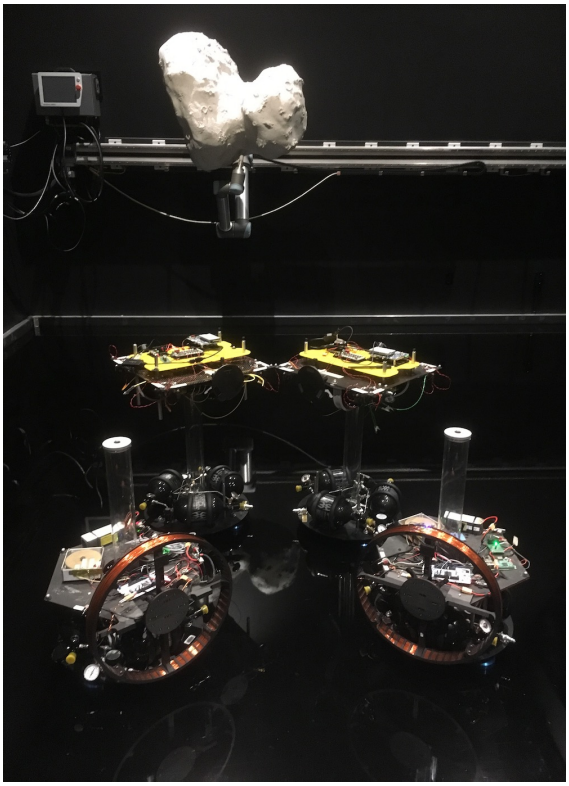

Fig. 1: Caltech's Spacecraft Simulator Facility and Four M-STARs with the Two Docking Systems

1.3 *Paper Overview and Organization*

This paper presents an electromagnet-based docking system capable of very low terminal velocity docking, which is ideal for in-orbit assembly applications. The mechanical design, control design, and experimental validation is presented and performance is compared against a thruster-based docking scheme.

The docking system for both electromagnets and thrusters is explained in Section 2. Secondly, the actuator models for both thrusters and electromagnets are shown in Section 3. Then, the control strategy

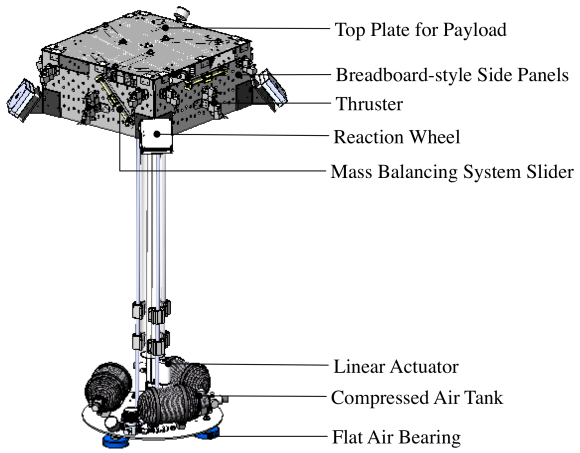

Fig. 2: M-STAR Spacecraft Simulator

is explained in Section 4. Experimental results and data analysis are presented in Section 5, ending with the conclusions in Section 6.

2 Docking System Overviews

2.1 *Electromagnet-based Docking*

The first docking system tested on the M-STARs is a custom electromagnet-based docking system. The system is shown in Fig. 3 and is mounted on the lower stage of the spacecraft simulator. The main components of the electromagnet-based docking system are: electromagnets, docking ports, reaction wheels, gyroscopes, batteries, and driving electronics.

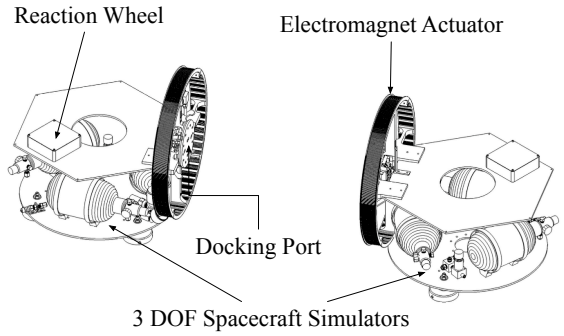

Fig. 3: Two 3DOF M-STARs Equipped with Electromagnets, Docking Ports, and Reaction Wheels

2.1.1 *Electromagnet Design*

The electromagnets are designed to provide a force of $f_{lim} = 40$ mN at 40 cm coil-to-coil distance and take up less than 20% of the entire mass of the spacecraft simulator including the structure and docking port. The number of windings, coil radius, coil thickness, and maximum current specifications are calculated using a Sequential Least Squares Programming optimization constrained to meet the above requirements while minimizing mass and power consumption.

$$\begin{aligned} \min_{N,l,R,i} \quad & c_1 p(N,l,R,i) + c_2 m(N,l,R) \\ \text{s.t.} \quad & f = f_{lim} \\ & m \leq m_{max} \\ & p \leq p_{max} \end{aligned}$$

The design of the electromagnet can be seen in Fig. 4. The coils were mounted on a 3D printed frame with cutouts to increase airflow and prevent overheating, which causes an increase in the resistance of the wire.

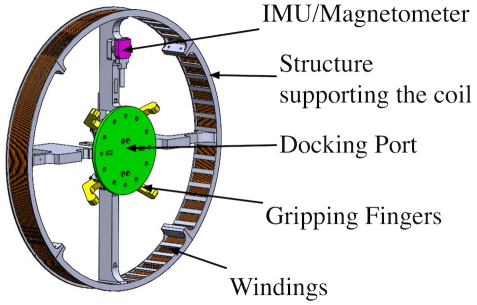

Fig. 4: Electromagnet Design

The electromagnet-based docking system runs a real-time current controller, shown in Fig. 5, to compensate for the induced voltage generated when the two spacecraft move with respect to each other. The feedback controller runs on the microcontroller at 1 kHz. The controller takes a current setpoint and outputs a drive voltage for the electromagnet, using feedback from a precise current sensor based on a low-tolerance shunt resistor.

2.1.2 *Reaction Wheel Design*

A reaction wheel for the heading control was custom designed to compensate for the torque generated by the electromagnets during docking and keep the two spacecraft oriented towards each other during the entire docking phase. Its specifications can be seen in Fig. 6. More detail on the reaction wheel design can be found in Ref. [25].

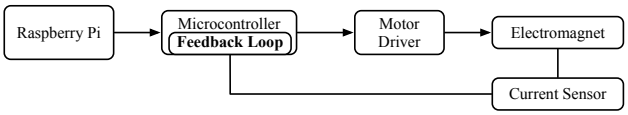

Fig. 5: Electromagnet Current Controller

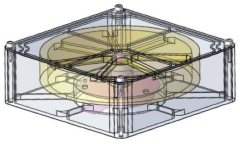

Angular momentum	0.12 Nms
Torque	0.010 Nm
Mass	0.52 kg
Volume	105 x 105 x 36 mm
Power	16 W
Cost	~ $1'500

Fig. 6: Custom Reaction Wheel Design and Specifications

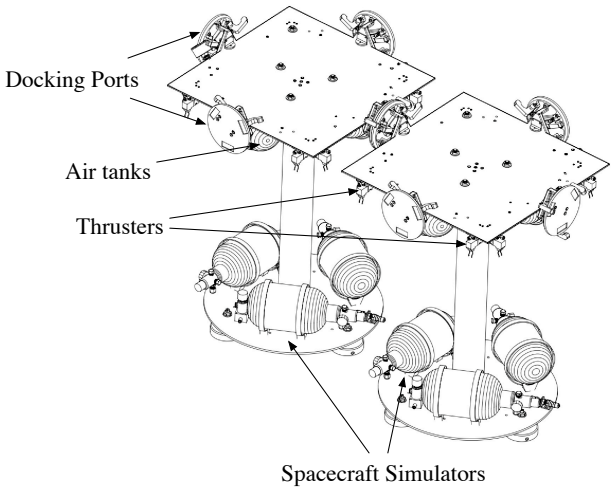

Fig. 7: Two M-STARs With Thrusters and Four Docking Ports

2.2 *Thruster-based Docking*

Thruster-based docking on the spacecraft simulators uses two 3DOF M-STARs, configured with a tube connecting the upper thruster stage with the lower stage. In Fig. 7, two docked 3DOF thruster M-STARs are shown. Each M-STAR has eight on-off solenoidal thrusters connected through a regulator to three compressed air cylinders, driving electronics, and four docking ports, presented in subsection 2.3, which are mounted on each side of spacecraft simulator upper stages. A more detailed description of the thruster system on-board the M-STARs can be seen in Ref. [25].

2.3 *Docking Port Design*

Once the spacecraft are moved into proximity by the electromagnets, a gripping mechanism has to ridigize the system and allow the magnets to be turned off. The gripping mechanism is designed to be androgynous, so any spacecraft can dock to any other, and to lock so that no torque is needed on the motor to keep the gripper in closed position.

The design of the docking port can be seen in Fig. 8. The servomotor in the center of the gripper connects to the fingers using push rods, which lock into place at the closed configuration so that once the gripper is closed, the motor can be turned off. Additionally, a high friction surface is added to the docking port's plate to constrain the rotational motion.

The reaction wheel should be able compensate for any heading error that happens between the spacecraft while docking, but the gripper can accommodate for misalignment as well. The misalignment was measured experimentally by putting the two spacecraft at a certain separation and measuring the offset before gripping. The maximum distance between the two grippers where the dock succeeds is 2 mm. The maximum lateral misalignment between the two grippers is 12 mm. These values can be improved by changing the finger shape but are sufficient for this work.

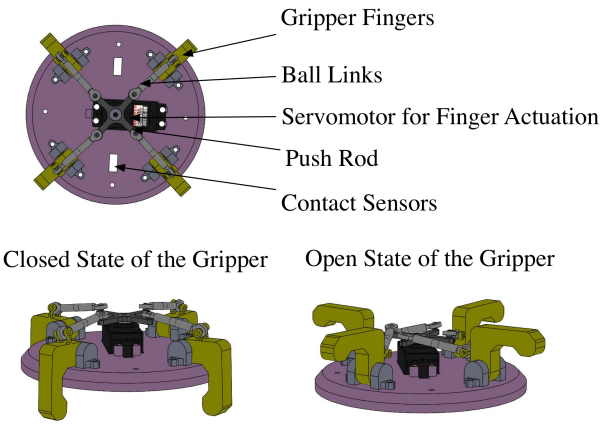

Fig. 8: Kinematics of the Gripper Mechanism

3 Actuator Models

3.1 *Electromagnet Model*

The force between two electromagnets is traditionally found using Ampere's Force Law, but in practice the numerical integration required is computationally costly, particularly for small distances. Additionally, the simplified Far-Field Model between two dipoles is inaccurate for docking applications, where the distance between the dipoles cannot be assumed insignificant with respect to the size of the dipoles. Therefore, analytical equations for the forces between coaxial and non-coaxial coils from Refs. [26, 27, 28] were used for the docking controller.

Given two cylindrical axisymmetric coils, the axial turn density for both coils assuming constant thickness is:

$$\sigma = \frac{N}{l} \quad [1]$$

For axisymmetric coils, $F_z = 0$ and the axial force can be expressed in terms of elliptical integrals and reduced to the following formula:

$$F_z = -\mu_0 i_1 i_2 R^2 \sigma^2 \int_0^{\pi} \chi(R,h) d\theta \quad [2]$$

where $\chi(r,h)$ and k are:

$$\chi(R,h) = \frac{1}{\pi}\frac{h}{r^2}\left(\frac{\mathbf{E}(\mathbf{k})}{k} - \frac{(h^2+4R^2)k\mathbf{K}(\mathbf{k})}{4R^2}\right) + \frac{1}{2} \quad [3]$$

$$k = \frac{2R}{\sqrt{4R^2+h^2}} \quad [4]$$

In Eq. 3, $\mathbf{K}(\mathbf{k})$ is the complete elliptic integral of the first kind, while $\mathbf{E}(\mathbf{k})$ is the complete elliptic integral of the second kind. The radial force is zero if the two spacecraft are aligned axially. In case of misalignment, their expressions can be seen in Eq. (34) from Ref. [28].

This electromagnet model gives good results assuming the attitude controller of each spacecraft simulator points them towards each other, so there are no side forces generated by the electromagnet. Therefore, the attitude of each of spacecraft must be accurately known. From several flown three-axis stabilized missions described in Refs. [29, 30], the attitude determination ranged from 0.001 to 3 degrees accuracy (1σ), depending on the sensors used on-board the spacecraft. Thus, this electromagnet model will give good results in real space applications.

3.2 *Thruster Model*

The M-STAR thrusters are solenoids firing high pressure breathable air from storage tanks on the upper stage. The solenoids have a response time of 10 ms during the energizing mode. The impulse generated by a valve multiplied by the minimum time between on and off states is called the MIB (I_{min}). This parameter is critical for a docking maneuver where very small forces need to be applied. The MIBs for the M-STAR thrusters was determined in prior work in Ref. [25] and are summarized in Table 2. This parameter is also used in control allocation.

Operating Pressure (psi)	Minimum Impulse (N-s)
40	0.0035
50	0.006
60	0.0075

Table 2: M-STAR MIB For Several Solenoid Operating Pressures, 20 ms Firing Time [25]

4 Control

For the feedback controllers on both docking systems, the pose and the angular velocity for each spacecraft were determined by the motion capture system in the flat floor facility and the on-board gyroscope. The dock finalization was also the same for both systems, with the gripper closing when the two satellites are touching.

4.1 *Trajectory Planner*

The trajectory that was input into both controllers is a constant acceleration profile. For electromagnet-based docking, an acceleration of 0.3 mm/s was input, while the velocity was limited to 45 mm/s. For thruster-based docking, the acceleration is 1 mm/s, while the velocity limit is infinity. After initial experiments, an advanced trajectory planner was implemented to allow four M-STARs to dock. More details on the trajectory planner can be found in Subsection 5.4.

4.2 *Electromagnet-Based Docking*

The electromagnet-based docking involves three controllers (Fig. 9). For attitude control, two PIDs in cascade are used, one that takes as input the heading and outputs an angular velocity, that is then fed into the second controller. For the distance control, a single PID was implemented. The input of the controller is the intersatellite distance. However, due to the non-linearity between the input and the output

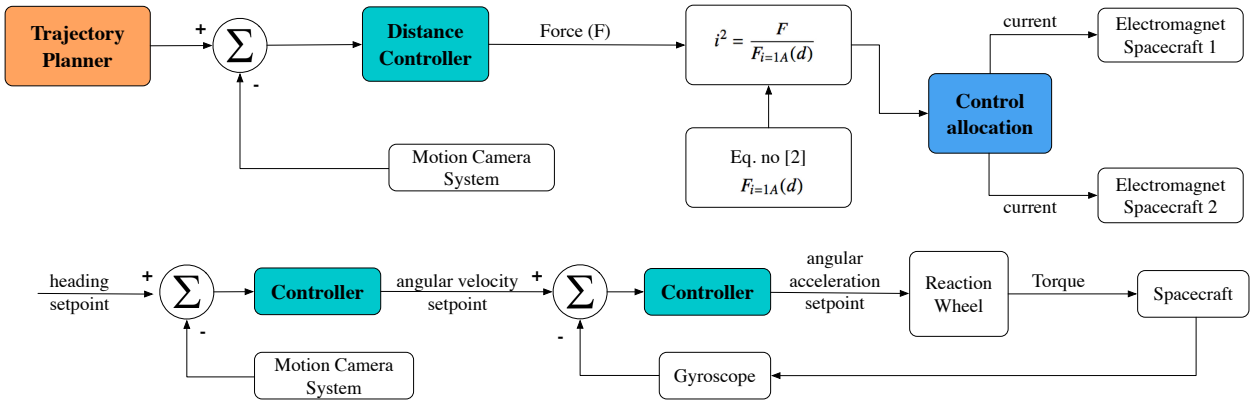

Fig. 9: Distance Controller for Electromagnet-based Docking System

(the current in the electromagnets), the gain of the PI controller will have drastically different effect at different distances. Thus, the controller determines the required force, which is used as a virtual input for an inverse input nonlinear function which determines the current that is input into the electromagnets. The poses of the two spacecraft simulators obtained from the motion capture system were used to determine the intersatellite distance and the heading error. The distance controller uses the distance between the electromagnets as a setpoint and controls the electromagnet forces.

The required currents for the two electromagnets are computed from the force output by the controller. The force at any distance is proportional to the product of the current (i) of the two coils. Therefore, using Eq. (5), the required current product can be computed from the force given for 1 Ampere ($F_{i=1A}$) computed using Eq. 2.

$$i_1 i_2 = \frac{F}{F_{i=1A}(d)} \quad [5]$$

The current is allocated between the two electromagnets using the following equations:

$$i_1 = \sqrt{|i_1 i_2|} \quad [6]$$

$$i_2 = sign(i_1 i_2)\sqrt{i_1 i_2} \quad [7]$$

One of the spacecraft was chosen to always have a positive current, while the second one was chosen to have the sign of the current product. In practical applications it may be preferable to have a control allocation scheme that trades between the two to prevent overheating.

4.3 *Thruster-Based Docking*

The thruster controller uses a PID in cascade with velocity feed-forward for position control and another PID for heading control. The controller determines the desired forces and moment that is then allocated to each individual thruster.

The forces and moment in body frame can be expressed as the follows:

$$\begin{bmatrix} f_x^B \\ f_y^B \\ m_z^B \end{bmatrix} = B\mathbf{F} \quad [8]$$

where $\mathbf{F}$ is the thrust vector and B is the control influence matrix defined as:

$$B = \begin{bmatrix} 1 & 1 & 1 & 1 & 0 & 0 & 0 & 0 \\ 0 & 0 & 0 & 0 & 1 & 1 & 1 & 1 \\ 1 & -1 & 1 & -1 & 1 & -1 & 1 & -1 \end{bmatrix} \quad [9]$$

The thruster control allocation is determined using the Moore-Penrose pseudoinverse of the control influence matrix.

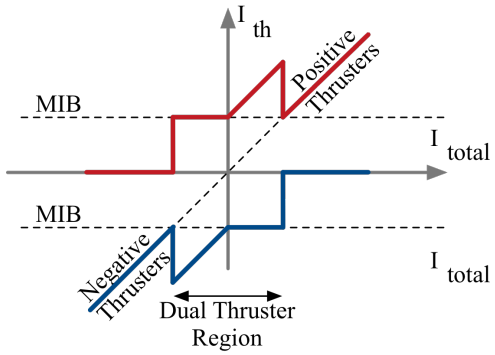

Fig. 10: Thruster Allocation Based on MIB

For fine velocity and position control where the total desired impulse for the spacecraft is less than the MIB allows, two counteracting thrusters are allocated. The allocation scheme for each of the pair of counteracting thrusters can be seen in Fig. 10. This function is designed in such a way that each thruster has either 0 or more than its minimum impulse.

In this manner, very small net forces can be applied on the spacecraft for precise docking. This solution is expensive in terms of propellant because two counteracting thrusters need to fire in the same time, thus it is only done for close-approach maneuvers when distance between the spacecraft simulators is less than 20 cm.

5 Results

Experimental validation of the two docking systems was performed in the flat floor facility at Caltech. Due to the design of the facility and the M-STARs, friction between the floor and the linear air bearings is small.

5.1 *Electromagnet-Based Docking*

Tests for the electromagnet-based docking system were performed by placing the two simulators a set distance apart, then starting the position and heading controllers. Several tests were performed by keeping the distance constant at approximately 40 cm apart. Afterwards, the initial intersatellite distance was increased in each test until the electromagnets could no longer attract enough to overcome the static friction of the floor. The maximum intersatellite distance was found to be 55 cm. The results at 55 cm distance are discussed below.

The real trajectory of the two simulators is shown in Fig. 11, with the heading angle shown as the orientation of miniaturized hexagons at various points along the trajectory. The final orientation and position of the two simulators is shown by the life-sized hexagons.

It is clear to see that the electromagnets have quite a bit of drift in heading, which could be caused by imbalances in the simulator mass or issues with the reaction wheel like vibrations. The system is still able to maintain relative alignment though, so the docking is still successful.

The control input is the current in each of the electromagnets, seen in Fig. 12. Note that because this experiment has the highest possible intersatellite distance, the current is saturated to 4.5A which is the maximum the electromagnets can reach with the power supply used in this experiment (a 5-cell lithium polymer battery). The current can be increased by using more power, wire with slightly less resistance than copper such as silver wire, or superconductors.

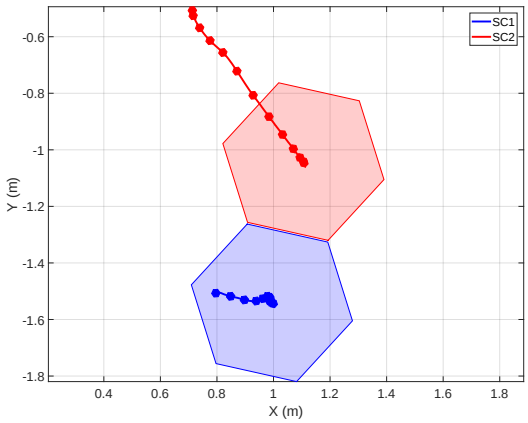

Fig. 11: Electromagnet-based Docking Trajectory with Orientation Represented using Hexagons

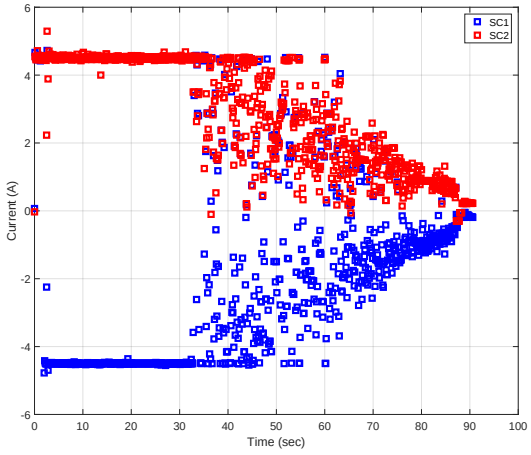

Fig. 12: Electromagnet Current Commanded vs. Time

The spacecraft point towards each other using the reaction wheel presented in Fig. 6. In Fig. 13, the angular momentum and torque of the reaction wheels are shown, while in Fig. 14, the heading of the two spacecraft is shown. The reaction wheel is saturating at 5000 rpm in this case.

The intersatellite distance tracking accuracy of the electromagnet-based docking system is shown in Fig. 15, which displays the standard deviation of the distance tracking error over time during the 14 test

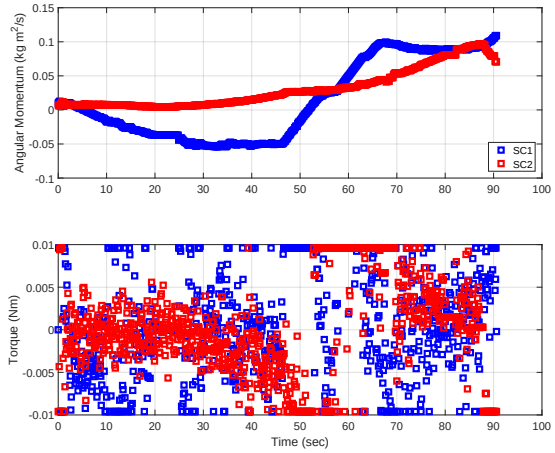

Fig. 13: Angular Momentum and Torque of the Reaction Wheel vs Time

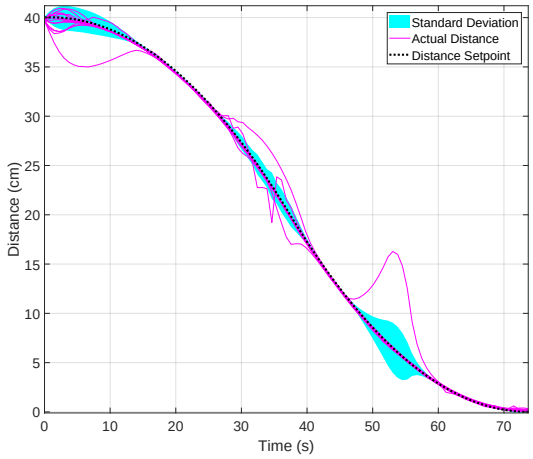

Fig. 15: Electromagnet-based Docking System Tracking Error

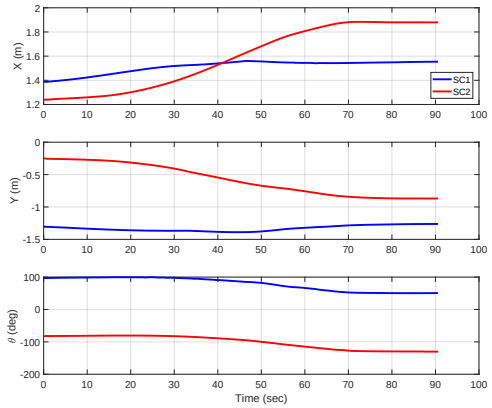

Fig. 14: X Y Position and Heading of the Two M-STARs vs Time

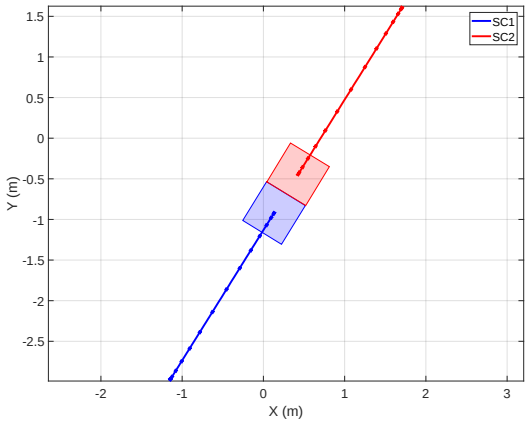

Fig. 16: Thruster Docking Trajectory with Orientation Represented using Squares

runs. It is seen that the controller is robust to position errors, as long as they are inside the attraction envelope of the electromagnet. The maximum standard deviation of the tracking error is 2.59 cm.

5.2 *Thruster-Based Docking*

Since the thrusters are not limited by intersatellite distance but by propellant consumption, these experiments all started from much higher separations. The trajectory resulting from one of thruster-based docking tests is shown in Fig. 16. During this test, the spacecraft were placed 5 meters apart. The components of the velocities of the two spacecraft can be seen in Fig. 18.

The resultant force for each of the positive and negative thrusters during translation phase is seen in Fig. 17. It is observed that the thrusters are not firing less than the time corresponding to the MIB, which is 16 ms.

Fig. 19 shows the trajectory tracking accuracy during 12 of the 14 thruster-based docking test runs. Two runs were excluded because the initial separation was significantly below the average. The maximum standard deviation of the tracking error is 4.17 cm.

5.3 *Experimental Results - Comparison*

The two analyzed docking systems are compared by evaluating the initial separation, final relative ve-

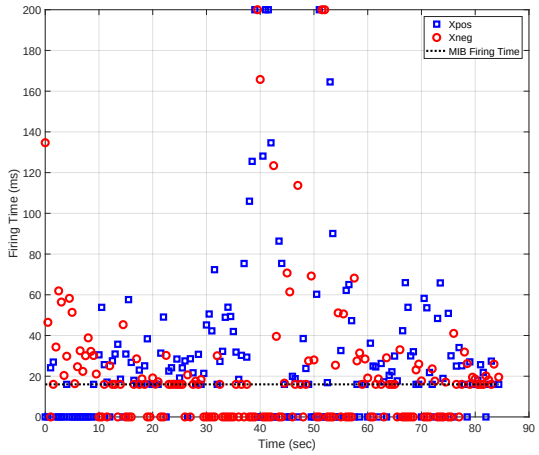

Fig. 17: MIB

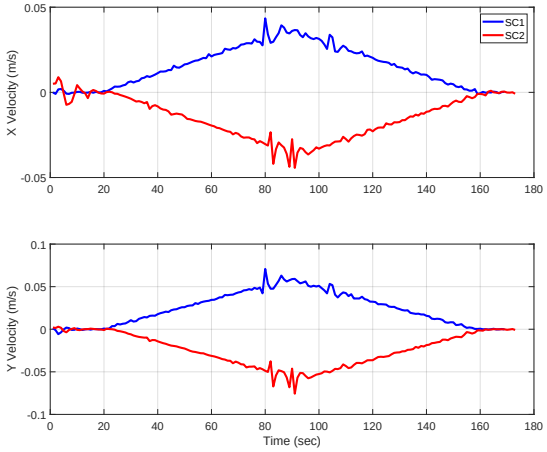

Fig. 18: X and Y Velocities vs Time

locity, consumable usage and docking success. Unlike other metrics, consumables are specific to each of the docking systems. For thruster-based docking, the total firing time of each of individual thrusters used for position and attitude control is computed. For electromagnet-based docking, the energy is computed as the average power multiplied by the docking time. The results from the two docking systems during the 14 tests are presented in the Tables 3 and 4 in Appendix A.

To assess the ultra-soft docking capability of both systems, in Figure 20, the relative velocity between the two spacecraft simulators is plotted. The thrusters perform well compared to the electromagnets, however, at the cost of significant propellant

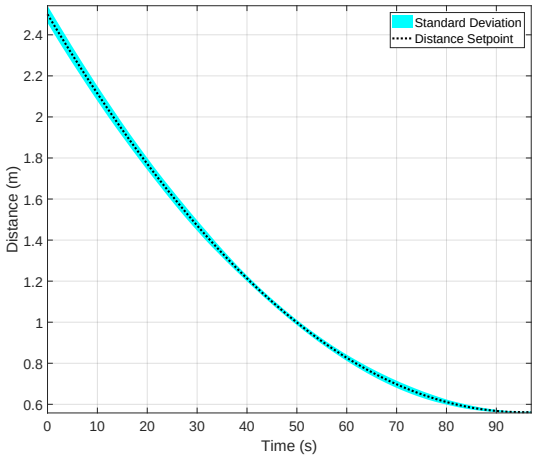

Fig. 19: Thruster-based Docking System Tracking Error

use. During the first 8 runs, the electromagnets had an erroneous offset of 2.5 mm, thus the relative velocity is artificially higher than subsequent runs where the error was corrected. After this issue was solved, it can be seen that the electromagnets are under the ultra-soft docking velocity limit (less than 1 mm/s). Additionally, in this plot it is shown that Test 5 is a failed dock. The spacecraft were not able to dock in this test due to the aforementioned offset and the fact that the gripper is designed to grip at a maximum separation of 2 mm. This was the only electromagnet-based docking test where the gripper did not ridigize the two spacecraft. For thruster docking, a dock failure occurred in Test 13, caused by a misalignment.

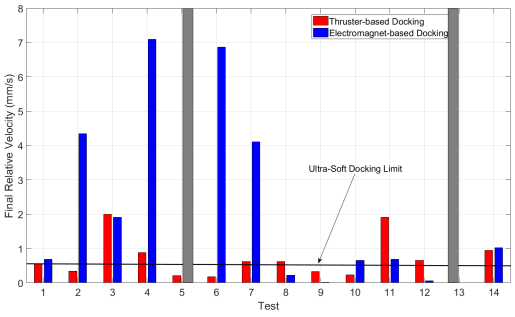

Fig. 20: Relative Velocity for the 14 runs

5.4 *In-Orbit Construction Experiment*

Once the docking methods were implemented and thoroughly tested, an in-orbit construction experi-

ment was designed. Using 4 M-STARs in the 3DOF, thruster-based docking configuration, a T shape was made in the center of a 4 meter square. Three of the four agents were identical, with two docking ports placed on opposite sides of the square upper stage. The fourth M-STAR had four ports, one on each side of the upper stage. These specifications were input into the Swarm Orbital Construction Algorithm [31, 32] to generate optimal, collision-free construction trajectories. Due to time limitations, the trajectories were computed offline then fed to the M-STARs, but the onboard implementation will be completed soon. These trajectories were then followed using the onboard control scheme described above.

Due to the aggressive nature of the optimal trajectories, the simulators come very close. Errors in trajectory tracking caused several initial attempts to fail. After extensive gain tuning and cleaning of the flat air bearings and the floor, the construction was successful and repeatable. A sample experimental trajectory is seen in Fig. 21. Links to videos for the three experiment types can be found in Appendix B.

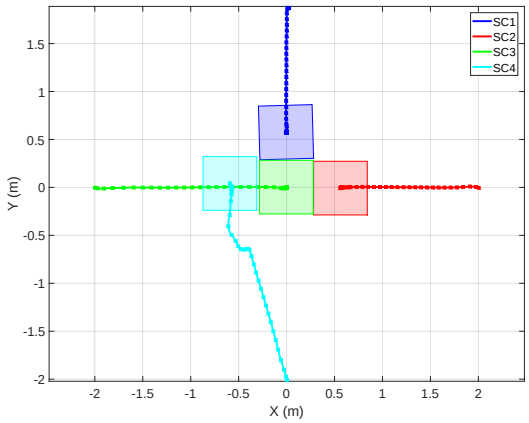

Fig. 21: 4 M-STARs Following SOCA Optimal Trajectories

6 Conclusion

Two docking systems were presented and experimentally validated. The electromagnet-based docking system performed admirably and was able to complete docks from up to a 55 cm intersatellite distance. The electromagnet-based docking system suffers from angular drift, most likely due to imbalances and manufacturing issues in the reaction wheels. The thruster-based docking system was able to successfully capture with a fairly low relative velocity but to achieve such a low velocity the propellant usage was high. Finally, four spacecraft simulators were used to experimentally validate an optimal construction algorithm. The trajectories from the algorithm resulted in all three docks succeeding. Work remains to isolate the potential error sources in the electromagnetic docking system to reduce the drift, incorporate on-board navigation to remove the reliance on the motion capture system, and redesign the gripper to improve robustness to misalignment.

7 Acknowledgements

The work of Rebecca Foust was supported by a NASA Space Technology Research Fellowship and in part by the Jet Propulsion Laboratory (JPL). Government sponsorship is acknowledged. The part of the work of Sorina Lupu was in fulfillment of the Swiss Federal Institute of Technology Master Thesis, coordinated by Professor Colin Jones.

The authors also thank Lorraine Fesq, Issa Nesnas, Marco Quadrelli, Adrian Stoica, Rashied Amini and Michael Wolf for their technical input.

The authors acknowledge the work done by Richard Eric Rasmussen in designing and constructing the spacecraft simulators. Thanks so much to our wonderful undergraduate students Jui Hung Sun for building the thruster experimental setup and designing version 1 of the thruster control board, David Elliot for improving the thruster control board and so much soldering, Asta Wu for optimizing the docking port design and constructing the ports, Karen Chen for helping with mechanical design of interfaces and Irene Crowell for creating a wonderful software architecture.

Appendix A: Experiment Analysis Tables

Test	Initial Separation Distance [m]	Final Relative Velocity [mm/sec]	Docking Time [sec]	Total Firing Time [sec]
1	1.99	0.56	61.00	31.79
2	4.00	-0.34	92.00	52.61
3	4.49	2.00	97.50	52.12
4	5.50	0.88	107.50	60.41
5	5.46	0.22	107.50	46.66
6	5.42	0.17	107.50	68.17
7	5.38	0.63	78.00	43.20
8	5.38	0.63	78.00	43.20
9	4.81	0.34	101.00	86.59
10	2.17	0.24	65.50	44.41
11	3.25	-1.92	81.50	70.86
12	4.50	0.66	96.50	67.39
13	4.50	0.66	96.50	67.39
14	1.06	-0.95	39.50	23.25

Table 3: Thruster-based Docking - Test Results

Test	Initial Separation Distance [m]	Final Relative Velocity [mm/sec]	Docking Time [sec]	Energy [Wh]
1	0.39	0.689	73.50	0.97
2	0.40	4.349	73.60	0.98
3	0.39	-1.911	73.20	0.95
4	0.39	7.093	73.50	0.97
5	0.38	0.000	72.60	0.92
6	0.38	6.867	72.29	0.95
7	0.40	4.103	73.90	1.00
8	0.40	-0.226	73.90	0.97
9	0.47	0.016	80.40	1.13
10	0.39	-0.651	72.80	0.95
11	0.39	0.689	73.50	0.85
12	0.40	0.065	74.10	0.90
13	0.41	0.003	74.90	0.86
14	0.55	1.019	87.10	1.34

Table 4: Electromagnet-based Docking - Test Results

Appendix B: Experiment Videos

Electromagnet-based Docking:
`https://youtu.be/q2t74AjeQE8`

Thruster-based Docking:
`https://www.youtube.com/watch?v=-k0IJelQVjk`

SOCA Validation:
`https://www.youtube.com/watch?v=62cngDR1k-E`

References

[1] S. Bandyopadhyay, R. Foust, G. P. Subramanian, S.-J. Chung, and F. Y. Hadaegh, "Review of formation flying and constellation missions using nanosatellites," *Journal of Spacecraft and Rockets*, no. 0, pp. 567–578, 2016.

[2] G. Bonin, N. Roth, S. Armitage, J. Newman, B. Risi, and R. E. Zee, "Canx–4 and canx–5 precision formation flight: Mission accomplished!," 2015.

[3] C. P. Bridges, B. Taylor, N. Horri, C. I. Underwood, S. Kenyon, J. Barrera-Ars, L. Pryce, and R. Bird, "Strand-2: Visual inspection, proximity operations amp;amp; nanosatellite docking," in *2013 IEEE Aerospace Conference*, pp. 1–8, March 2013.

[4] M. Nohmi, "Mission design of a tethered robot satellite "stars" for orbital experiment," in *2009 IEEE Control Applications, (CCA) Intelligent Control, (ISIC)*, pp. 1075–1080, July 2009.

[5] M. Nohmi, "Initial orbital performance result of nano-satellite stars-ii," in *Proceedings of the 2014 International Symposium on Artificial Intelligence, Robots and Automation in Space*, 2014.

[6] J. Bowen, A. Tsuda, J. Abel, and M. Villa, "Cubesat proximity operations demonstration (cpod) mission update," in *2015 IEEE Aerospace Conference*, pp. 1–8, March 2015.

[7] "Rascal-1: A do-si-do in space." `https://www.sluspacelab.com/slu04-rascal1/`, 2018. Saint Louis University SSRL. Accessed 2018-02-15.

[8] "Cleanspace one." `https://espace.epfl.ch/CleanSpaceOne_1`, 2018. EPFL Space Engineering Center eSpace. Accessed: 2018-01-30.

[9] S. Nolet and D. W. Miller, "Autonomous docking experiments using the spheres testbed inside the iss," in *Sensors and Systems for Space Applications in Defense and Security Symposium*, vol. 6555, SPIE, 2007.

[10] J. Bonometti, "Boom Rendezvous Alternative Docking Approach," in *Space 2006*, pp. 1–13, 2006.

[11] W. Fehse, *Automated rendezvous and docking of spacecraft*, vol. 16. Cambridge university press, 2003.

[12] R. C. Foust, Y. K. Nakka, A. Saxena, S.-J. Chung, and F. Y. Hadaegh, "Automated rendezvous and docking using tethered formation flight," in *9th International Workshop on Satellite Constellations and Formation Flying*, 2017.

[13] S.-J. Chung, J.-J. E. Slotine, and D. W. Miller, "Nonlinear model reduction and decentralized control of tethered formation flight," *Journal of Guidance, Control, and Dynamics*, vol. 30, no. 2, pp. 390–400, 2007.

[14] S.-J. Chung, *Nonlinear control and synchronization of multiple Lagrangian systems with application to tethered formation flight spacecraft*. PhD thesis, Massachusetts Institute of Technology, 2007.

[15] O. Mori and S. Matunaga, "Formation and attitude control for rotational tethered satellite clusters," *Journal of Spacecraft and Rockets*, vol. 44, no. 1, pp. 211–220, 2007.

[16] L. Olivieri, R. Mantellato, F. Branz, F. Sansone, A. Cavinato, M. Gaino, D. Petrillo, A. Francesconi, and E. C. Lorenzini, "Cubesat mission concept for tethered electromagnetic docking demonstration," in *Tartu Conference on Space Science and Technology*, 2014.

[17] D. Petrillo, M. Buonomo, A. Cavinato, F. Chiariotti, M. Gaino, F. Branz, R. Mantellato, L. Olivieri, F. Sansone, A. Francesconi, *et al.*, "Flexible electromagnetic leash docking system (felds) experiment from design to microgravity testing," in *66th International Astronautical Congress*, 2015.

[18] M. Duzzi, L. Olivieri, and A. Francesconi, "Tether-aided spacecraft docking procedure," 4S Symposium, 2016.

[19] J. Pei, L. Murchison, V. Stewart, J. Rosenthal, D. Sellers, M. Banchy, A. BenShabat, R. Elandt, D. Elliott, and A. K. Weber, "Autonomous rendezvous and docking of two 3u cubesats using a novel permanent-magnet docking mechanism," in *54th AIAA Aerospace Sciences Meeting*, 2016.

[20] S. Schweighart, *Electromagnetic Formation Flight Dipole Solution Planning*. PhD thesis, Massachusetts Institute of Technology, 2005.

[21] E. M.-C. Kong, *Spacecraft Formation Flight Exploiting Potential Fiels*. PhD thesis, Massachusetts Institute of Technology, 2002.

[22] U. Ashun, *Dynamics and Control of Electromagnetic Satellite Formations*. PhD thesis, Massachusetts Institute of Technology, 2007.

[23] D. W. Kwon, *Cryogenic Heat Pipe for Cooling High Temperature Superconductors with Application to Electromagnetic Formation Flight Satellites*. PhD thesis, Massachusetts Institute of Technology, 2009.

[24] L. Jones and M. A. Peck, "Stability and Control of a Flux-Pinned Docking Interface for Spacecraft," in *AIAA Guidance, Navigation, and Control Conference*, pp. 1–12, 2010.

[25] Y. K. Nakka, R. C. Foust, E. S. Lupu, D. B. Elliott, I. S. Crowell, S.-J. Chung, and F. Y. Hadaegh, "Six degree-of-freedom spacecraft dynamics simulator for formation control research," in *2018 AAS/AIAA Astrodynamics Specialist Conference*, 2018.

[26] R. Ravaud, G. Lemarquand, S. Babic, V. Lemarquand, and C. Akyel, "Cylindrical magnets and coils: Fields, forces, and inductances," *IEEE Transactions on Magnetics*, vol. 46, pp. 3585–3590, Sept 2010.

[27] W. Robertson, B. Cazzolato, and A. Zander, "A Simplified Force Equation for Coaxial Cylindrical Magnets and Thin Coils," *IEEE Transactions on Magnetics*, vol. 47, no. 8, pp. 2045–2049, 2011.

[28] J. T. Conway, "Forces Between Thin Coils With Parallel Axes Using Bessel Functions," *IEEE Transactions on Magnetics*, vol. 49, no. 9, pp. 5028–5034, 2013.

[29] S.-J. Chung, S. Bandyopadhyay, R. Foust, and G. Subramanian, "Review of Formation Flying and Constellation Missions Using Nanosatellites," *Journal of Spacecraft and Rockets*, vol. 53, no. 3, 2016.

[30] D. Brasoveanu and J. Hashmall, "Spacecraft attitude determination accuracy from mission experience," *Flight Mechanics/Estimation Theory Symposium*, 1994.

[31] R. Foust, S.-J. Chung, and F. Y. Hadaegh, "Real-time optimal control and target assignment for autonomous in-orbit satellite assembly from a modular heterogeneous swarm," in *26th AAS/AIAA Space Flight Mechanics Meeting, Napa, CA, February 14-18, 2016*.

[32] R. Foust, S.-J. Chung, and F. Hadaegh, "Autonomous in-orbit satellite assembly from a modular heterogeneous swarm using sequential convex programming," in *AIAA/AAS Astrodynamics Specialist Conference, AIAA SPACE and Astronautics Forum and Exposition, Long Beach, CA, Sept. 13-16, 2016*.